EES Solar

PAPER

View Article Online
View Journal | View Issue

Cite this: *EES Sol.*, 2025, **1**, 839

Critical role of oxide anchoring groups in organic electron transport layers for perovskite solar cell stability

Sanggyun Kim, [a] Justine S. Wagner, [b] Sina Sabury, [b] Jack Lawton, [a] Martin Gómez-Domínguez, [a] Diana K. LaFollette, [a] Dwanleen E. Shen, [b] Anna M. Österholm, [b] Ruipeng Li, [c] Carlo A. R. Perini, [a] John R. Reynolds *[ab] and Juan-Pablo Correa-Baena *[ab]

Charge transport layers (CTLs) play a critical role in the performance and long-term stability of perovskite solar cells (PSCs) by facilitating efficient charge extraction and providing interfacial stabilization. For organic CTLs, different functional groups have been designed to modulate the interactions with the substrate. Anchoring groups are used to establish strong adhesion to transparent conductive oxides (TCOs) but are not routinely incorporated in organic CTL design. In this study, we investigate the influence of anchoring groups in organic electron transport layers (ETLs) on PSC performance and stability by synthesizing and evaluating two naphthalene diimide (NDI)-based ETLs: NDI-$(PhPA)_2$, functionalized with polar phenyl phosphonic acid (PhPA) groups, and NDI-$(PhBr)_2$, modified with nonpolar bromophenyl (PhBr) groups. X-ray photoelectron spectroscopy confirms that PhPA functionalization leads to NDIs anchored onto fluorine-doped tin oxide (FTO) following chemical bath deposition, while NDI-$(PhBr)_2$ shows no detectable surface presence after deposition. We show that NDI-$(PhPA)_2$ deposits as a thin film on FTO, exhibiting strong adhesion, high solvent resistance, and enhanced light and thermal stability, achieving a maximum device efficiency of 14.3%. Stability assessments conducted under continuous illumination at 25 °C for 200 hours and at 65 °C for 100 hours demonstrate performance on par with TiO_2-based ETLs. In contrast, NDI-$(PhBr)_2$, which lacks strong anchoring interactions, fails to adhere to the FTO surface, resulting in a rapid decrease in efficiency over a few hours, comparable to devices without an ETL. These findings highlight the importance of anchoring groups in organic CTLs for achieving long-term PSC stability under operational conditions.

Received 6th May 2025
Accepted 3rd August 2025

DOI: 10.1039/d5el00070j

rsc.li/EESSolar

Broader context

Metal halide perovskites (MHPs) are among the most promising materials for low-cost, high-efficiency optoelectronic technologies, including solar cells, photodetectors, and light-emitting devices. However, their widespread deployment remains hindered by device instability and poor interfacial durability, especially when using organic charge transport layers deposited *via* scalable methods. Although significant progress has been made in engineering hole transport layers with anchoring functionalities, the development of robust organic electron transport layers (ETLs) remains a major challenge due to weak interfacial adhesion and insufficient stability under operational conditions. This work addresses these limitations by introducing phosphonic acid-functionalized naphthalene diimides (NDIs) as ETLs for perovskite solar cells. By leveraging strong interfacial binding through phosphonic acid anchoring groups, these molecules form stable interlayers at the transparent electrode interface. We demonstrate that these materials enable enhanced wettability, superior film quality, efficient charge extraction, and long-term device stability under thermal and continuous illumination stress. These findings contribute to the broader goal of achieving durable and high-performing perovskite optoelectronics through molecular-level design of functional interlayers.

Introduction

Hybrid organic–inorganic perovskite solar cells (PSCs) have gained significant attention as next-generation photovoltaics due to their high-power conversion efficiency (PCE) and cost-effectiveness.[1–5] However, their long-term operational stability remains a significant challenge, limiting their commercial viability.[6–9] In particular, charge transport layers (CTLs) and their interactions with both the perovskite absorber and metal

[a]*School of Materials Science and Engineering, Georgia Institute of Technology, Atlanta, Georgia 30332, USA. E-mail: jreynolds43@gatech.edu; jpcorrea@gatech.edu*
[b]*School of Chemistry and Biochemistry, Center for Organic Photonics and Electronics, Georgia Institute of Technology, Atlanta, Georgia, 30332, USA*
[c]*National Synchrotron Light Source II, Brookhaven National Lab, Upton, New York, 11973, USA*

electrodes play a critical role in determining PSC stability.[10,11] CTLs serve as the intermediates between the perovskite absorber and electrodes, facilitating efficient charge extraction, minimizing recombination losses, and ensuring interfacial stability.[10,12,13] Instabilities within these interlayers are primarily attributed to mechanical cracking, delamination, ion migration, and interfacial chemical reactions, which compromise both structural integrity and electronic properties, leading to device degradation.[10,14,15] Therefore, the development of novel CTLs and strategic molecular design approaches is essential to enhance long-term stability.

Organic CTLs have emerged as promising candidates due to their solution processability, low-temperature fabrication, and tunable optoelectronic properties.[16] However, one of the key challenges in organic CTLs lies in achieving strong interfacial adhesion with transparent conductive oxides (TCOs) such as indium-doped tin oxide and fluorine-doped tin oxide (FTO) which are widely used as transparent electrodes in optoelectronic technologies.[15,17,18] Unlike metal-oxide based CTLs such as TiO_2 and SnO_2, which readily form chemical bonds with TCOs, organic CTLs often exhibit weak adhesion when the conjugated core itself lacks functional groups capable of directly binding to metal oxides. This can result in delamination and create discontinuities that hinder efficient charge transport, ultimately compromising device performance. To overcome these limitations, organic CTLs are commonly functionalized with anchoring groups, which facilitate strong interfacial bonding with the underlying TCOs as well as strong interaction with the perovskite layer. These anchoring groups play a decisive role in interfacial stabilization and indirectly improve charge transport by promoting uniform molecular coverage and reducing interfacial defects between TCOs and organic CTLs.[19,20]

Historically, achieving uniform and stable organic CTLs has been challenging due to poor adhesion to metal oxides and chemical incompatibility with perovskite precursor solutions. Various anchoring groups including carboxylic acids,[21] thiols,[22] alcohols[23], organosilanes,[24] and phosphonic acids (PAs)[20,25,26] have been explored, not only to strengthen interfacial bonding with TCOs, but also to modulate work function and tune surface energy, thereby enhancing charge extraction and controlling perovskite nucleation and film formation. Among these, PAs have demonstrated strong surface binding and self-assembled monolayer formation, making them particularly effective for stabilizing organic CTLs. Their strong adhesion primarily arises from bidentate or tridentate coordination of the PA group to metal atoms on the TCO surface, forming stable bonds.[25] Secondary hydrogen bonding with surface hydroxyl groups further reinforces these interactions, collectively promoting uniform film formation and enhancing interfacial stability between the TCO and the organics. PA-based anchoring has been widely implemented in organic hole transport layers (HTLs) for p–i–n PSC device architecture where molecules such as, [(2-(4-(bis(4-methoxyphenyl)amino)phenyl)-1-cyanovinyl) phosphonic acid (MPA-CPA) and 4-(7H-dibenzo[c, g]carbazol-7-yl)phenyl)phosphonic acid (Bz-PhpPACz) have displayed PCEs exceeding 24% with improved thermal stability.[27,28] For both molecules, the formation of a bi-layer, and the presence of phosphonic groups pointing towards the perovskite interface enhancing wettability were instrumental in driving the high performance. While these design strategies have been well established for HTLs, the use of PA-based anchoring groups in organic electron transport layers (ETLs) remain largely unexplored. To date, the only reported organic ETL in n–i–p PCS device with PA is *N*-(2,5-di-*tert*-butylphenyl)-*N*′-(methyl)-1,4,5,8-naphthalene tetracarboxylic diimide phosphonic acid (PANDI), which incorporates a single PA anchoring group and has demonstrated a PCE of 21.5%.[29] This limited precedent highlights the need for further systematic development of PA-functionalized organic ETLs to fully understand their potential in interfacial engineering, charge transport, and long-term device stability.

In this work, we examined two functionalized naphthalene diimide (NDI) based molecules as ETLs in n–i–p PSC device configuration, ((1,3,6,8-tetraoxo-1,3,6,8-tetrahydrobenzo[lmn][3,8]phenanthroline-2,-diyl)bis(4,1-phenylene))bis(phosphonic acid) (NDI-$(PhPA)_2$) which features PA group on each end of the molecule, and 2,7-bis(4-bromphenyl)benzo[lmn][3,8]phenanthroline-1,3,6,8(2H, 7H)-tetraone (NDI-$(PhBr)_2$), which has bromine terminations instead of the PA anchoring groups (Fig. 1a). NDI derivatives are widely recognized for their strong electron-accepting characteristics, high stability under ambient conditions, and efficient π–π stacking interactions to facilitate enhanced charge transport, making them attractive candidates for organic ETLs.[30–32] NDI-$(PhPA)_2$ was specifically designed to form robust covalent bonds with the TCO while providing enhanced surface hydrophilicity through its second PA group, thereby improving the wettability and uniform coverage of the perovskite layer. In contrast, NDI-$(PhBr)_2$ serves as a control to isolate the effect that the absence of PA groups have on adhesion. NDI-$(PhBr)_2$ relies solely on weak physisorption and lacks specific binding interactions with the TCO. Devices incorporating NDI-$(PhPA)_2$ demonstrate a maximum PCE of 14.3% and exhibit remarkable operational stability, retaining performance under continuous illumination at 25 °C for 200 hours and at 65 °C for 100 hours, comparable to devices using conventional TiO_2-based ETLs. Conversely, devices treated with NDI-$(PhBr)_2$ degrade rapidly, with performance indistinguishable from devices lacking an ETL. These results underscore the critical importance of anchoring group design in organic ETLs and establish PA functionalization as a highly effective strategy for achieving robust interface engineering and long-term device stability in PSCs.

Results & discussion

Synthesis and characterization of NDI-$(PhPA)_2$ & NDI-$(PhBr)_2$ molecules

The molecular structures of NDI-$(PhPA)_2$ and NDI-$(PhBr)_2$ are shown in Fig. 1a, with synthesis detailed in Fig. S1 and S8, and structural confirmation provided by nuclear magnetic resonance (NMR) spectroscopy (Fig. S2–S7 and S9–S13). Given that perovskite films are annealed at 150 °C during fabrication and device thermal stability assessments are conducted at 65 °C or

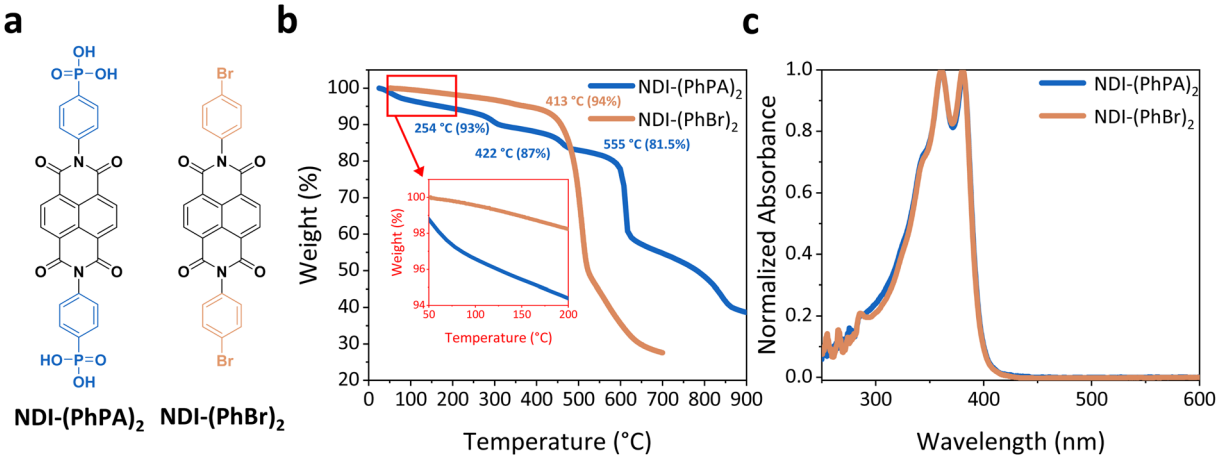

Fig. 1 Molecular structure, thermal stability, and optical property of NDI-based ETLs. (a) Molecular structure, (b) thermogram, and (c) normalized solution UV-vis absorption spectra of NDI-$(PhPA)_2$ and NDI-$(PhBr)_2$ molecules.

85 °C, both NDI-$(PhPA)_2$ and NDI-$(PhBr)_2$ need to remain structurally intact under standard PSC fabrication and operational conditions. To assess the thermal stability of these molecules, thermogravimetric analysis (TGA) was conducted on the powders (Fig. 1b), revealing distinct thermal behaviors. NDI-$(PhPA)_2$ exhibited three mass loss onsets at 254 °C, 422 °C, and 555 °C, indicating stepwise loss of different molecular components. In contrast, NDI-$(PhBr)_2$ displayed a single sharp mass loss onset at 413 °C, demonstrating a more thermally stable molecular framework compared to NDI-$(PhPA)_2$. The presence of mass loss onsets in NDI-$(PhPA)_2$ at a lower temperature than for NDI-$(PhBr)_2$ suggests an increased thermal instability introduced by the presence of the phosphonic acid groups. The absence of multiple decomposition steps indicates that NDI-$(PhBr)_2$ maintains its chemical structure until a critical thermal threshold is reached, at which point either degradation or molecular evaporation occurs. Both molecules exhibited initial decomposition temperatures well above 250 °C, indicating sufficient thermal stability for PSC processing and operation as shown in the inset of Fig. 1b. This thermal robustness is particularly significant, as degradation at the CTL interface can lead to device instability and efficiency losses.[33] Fig. 1c displays the normalized solution UV-vis absorption spectra of NDI-$(PhPA)_2$ and NDI-$(PhBr)_2$ in dimethyl sulfoxide (DMSO). Both molecules exhibit identical spectral shapes and absorptions onsets, characteristic of the NDI-core structure, with pronounced maxima at 361 nm and 381 nm.[34] The absence of absorption in the visible region is beneficial for light absorption by the perovskite active layer.

Examination of NDI-$(PhPA)_2$ and NDI-$(PhBr)_2$ thin films

Thin films of NDI-$(PhPA)_2$ and NDI-$(PhBr)_2$ were fabricated *via* chemical bath deposition (CBD), with the deposition durations optimized to maximize surface coverage (Fig. 2). Prior to film fabrication, the solubility of both molecules was evaluated at a concentration of 0.5 mg mL^{-1} in solvents of varying polarities, including chlorobenzene (CB, polarity = 0.188), DMSO (polarity = 0.444), and methanol (MeOH, polarity = 0.762), with polarity values referenced to H_2O (polarity = 1).[35] Both NDI-$(PhPA)_2$ and NDI-$(PhBr)_2$ were insoluble in CB and MeOH, while readily dissolving in DMSO. NDI-$(PhPA)_2$ dissolved fully at room temperature, whereas NDI-$(PhBr)_2$ required sustained heating at 100 °C to achieve complete dissolution. Based on these results, a concentration of 0.5 mg mL^{-1} in DMSO at 100 °C was selected for CBD processing. Following deposition, unbound molecules were removed by dipping the substrates in ethanol (EtOH). The films were then thermally annealed at 120 °C for 10 minutes to eliminate residual solvent.

Thin-film formation was optimized by varying the time of the CBD process for each molecule based on their anticipated interactions with the FTO surface. For NDI-$(PhPA)_2$, deposition times of 24, 48, and 72 hours were explored, as the anchoring group was expected to form strong chemical bonds with metal oxides, potentially enhancing film growth with extended deposition time. Conversely, NDI-$(PhBr)_2$, being nonpolar and dependent on weak physisorption to the metal oxide surface, was deposited over shorter durations of 6, 12, and 24 hours. Longer deposition times were not expected to improve coverage, as weak, non-specific interactions typically reach equilibrium rapidly and do not benefit from extended exposure, making shorter deposition times sufficient to assess any potential adsorption behavior.[36] Preliminary confirmation of molecular deposition and structural integrity was carried out by comparing thin-film UV-vis absorption spectra with solution-phase spectra (Fig. S16a and b). Thin films were deposited on glass substrates using the longest CBD durations, and spectra were acquired with a double-beam spectrophotometer, using a blank glass substrate as the reference to ensure that the recorded signals correspond exclusively to the deposited molecules. Both NDI-coated glass substrates exhibit an absorption at 260 nm and 270 nm, likely originating from minor baseline deviations arising from changes in the refractive index of the glass surface following CBD treatment.

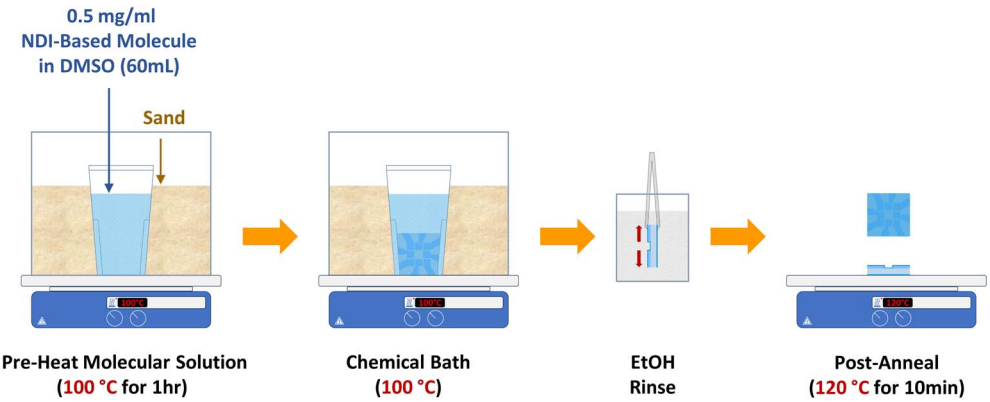

Fig. 2 CBD process of NDI-based ETLs. Schematic representation of the CBD process of NDI-based thin films.

Normalized thin-film spectra of NDI-$(PhPA)_2$ show distinct absorption peaks at 361 nm and 381 nm, matching those observed in solution, confirming deposition and preservation of molecular structure. In contrast, no corresponding peaks for NDI-$(PhBr)_2$ were observed, indicating the likely absence of film formation. As a result, only the optical HOMO–LUMO gap of NDI-$(PhPA)_2$ was determined using the Tauc method from the absorption edge between 370 nm and 390 nm, yielding a value of approximately 3.12 eV (Fig. S16c). In addition, absorptance spectra derived from transmittance and reflectance measurements further confirm that the lack of a defined band edge in NDI-$(PhBr)_2$ is not due to light scattering, and is instead due to the absence of any NDI-$(PhBr)_2$ on the substrate surface (Fig. S17).

X-ray photoelectrons spectroscopy (XPS) was performed to confirm the deposition of NDI-$(PhPA)_2$ and NDI-$(PhBr)_2$ onto the FTO substrates, and to assess the influence of varying chemical bath durations on molecular coverage. Fig. 3a and b present elemental XPS scans of P 2p and Br 3d, corresponding to NDI-$(PhPA)_2$ and NDI-$(PhBr)_2$ thin films, respectively. For

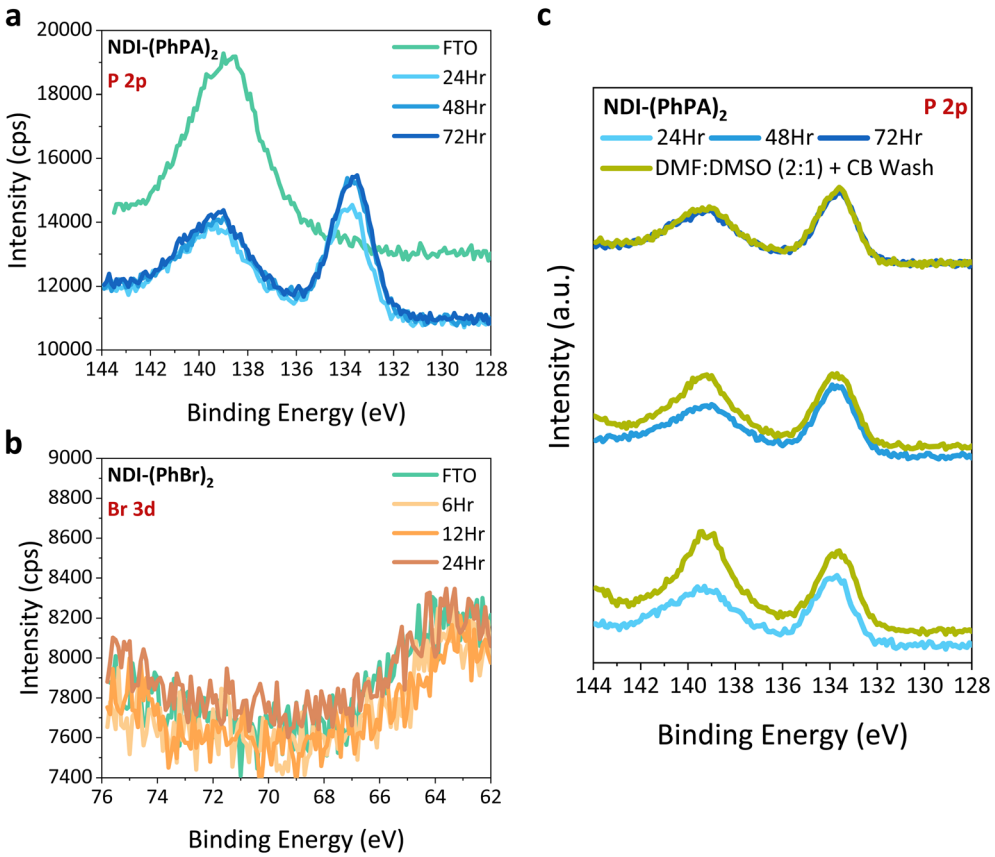

Fig. 3 XPS analysis of NDI-based ETLs on FTO. XPS spectra of (a) P 2p for NDI-$(PhPA)_2$ and (b) Br 3d for NDI-$(PhBr)_2$, deposited on FTO substrates under varying chemical bath durations. (c) XPS spectra of P 2p for NDI-$(PhPA)_2$ on FTO substrate, before and after washing with DMF : DMSO (2 : 1) and CB solvents, simulating the perovskite spin-coating conditions to assess molecular retention.

NDI-$(PhPA)_2$, P 2p signals were examined at chemical bath durations of 24, 48, and 72 hours, with bare FTO serving as a reference. The bare FTO exhibited a peak at 139 eV, which we could attribute it to Zn or Pb impurities from substrate processing. After NDI-$(PhPA)_2$ deposition, two distinct peaks with binding energies of 139 eV and 133.5 eV were observed. The persistent 139 eV signal, though reduced in intensity, is attributed to the underlying FTO substrate, whereas the new peak at 133.5 eV peak corresponds to phosphorous P 2p within the NDI-$(PhPA)_2$ molecule. The increasing signal intesity at 133.5 eV from 24 to 48 hours, followed by saturation between 48 and 72 hours, indicates progressive and self-limited deposition and suggests a monolayer is formed after this wait time. The deposition was further confirmed by a π–π^* satellite feature near 291.5 eV (Fig. S18) in the C 1s spectrum, which is attributed to the conjugated or aromatic π-electron systems in the NDI backbone.

For NDI-$(PhBr)_2$, the Br 3d signal was analyzed for samples processed at 6, 12, and 24 hours. No Br 3d signal was detected at any deposition duration, indicating the absence of measurable film formation. This result suggests that weak physisorption of the nonpolar PhBr groups and the hydroxyl-terminated FTO surface prevents stable adsorption, with any loosely adhered molecules likely removed during the EtOH dipping step of the CBD process. Consistent with this finding, the C 1s spectrum of NDI-$(PhBr)_2$ showed no π–π^* satellite feature (Fig. S19), and no N 1s signal was detected (Fig. S20). In contrast, N 1s peaks were clearly observed for NDI-$(PhPA)_2$, with increasing intensity correlating with longer deposition times, further supporting the formation of a uniform, well-anchored thin film. The absence of both Br 3d and N 1s signals for NDI-$(PhBr)_2$ conclusively confirms that stable film formation was not attained under the investigated conditions.

Effect of perovskite processing solvents on NDI-$(PhPA)_2$

To evaluate how much of the NDI-$(PhPA)_2$ molecules remain on the FTO substrates during perovskite deposition, polar and nonpolar solvents were spin coated on the ETL films (referred to in this paper as a "wash test"). The wash test was conducted to simulate the solvent environment encountered during the perovskite spin-coating process. This was achieved by sequentially spin-coating a 90 μL solution of dimethylformamide (DMF) and DMSO in a 2 : 1 volume ratio, followed by 250 μL CB onto as-cast thin films. Since DMSO, the solvent used in the CBD, is also used in the perovskite precursor solution, this test was designed to assess whether the NDI-$(PhPA)_2$ molecules remain adhered to the FTO surface under conditions relevant to PSC fabrication. Given that NDI-based molecules were initially deposited from DMSO during CBD, their ability to withstand this solvent exposure is critical for maintaining interfacial stability in PSCs.

For NDI-$(PhPA)_2$ thin films, XPS analysis revealed an increase in the signal at 139 eV following the wash test when compared to unwashed films (Fig. 3c), except for 72-hours depositions. The data shows an increase in the FTO signal after washing, suggesting that some of the NDI-$(PhPA)_2$ is being removed. This increase was inversely correlated with CBD duration, where the peak intensity increase at 139 eV was more pronounced for thin films deposited for 24 and 48 hours but remained largely unchanged for 72-hours depositions. These observations suggest that longer CBD durations enhance interfacial bonding. The ability of NDI-$(PhPA)_2$ to endure both polar DMSO and nonpolar CB solvent exposure is indicative of its stability under perovskite processing conditions, highlighting it as a suitable ETL for n–i–p PSCs. This illustrates the critical role of anchoring groups such as phosphonic acids in establishing strong interactions with metal oxides. Furthermore, the ability of NDI-$(PhPA)_2$ to withstand exposure to perovskite precursor solvents, particularly DMSO which was originally used for CBD, ensures interfacial integrity during PSC fabrication.

Photovoltaic performance

The effect of anchoring groups on PSC performance was explored by using n–i–p structured devices consisting of FTO/ETL/$Cs_{0.09}FA_{0.91}PbI_3$ perovskite/phenethylammonium iodide (PEAI)/doped spiro-OMeTAD/Au (Fig. 4a), where the ETL consisted of either NDI-$(PhPA)_2$ or FTO substrates subjected to CBD treatment with NDI-$(PhBr)_2$. Based on the XPS and washing results, devices processed with a 72-hours CBD time are considered for the subsequent device fabrication and characterization discussion (Fig. 4b). However, other deposition conditions were also explored and are reported in Fig. S21–S23 and Table S1–S3. Devices treated with NDI-$(PhBr)_2$ displayed modest performance improvement with respect to NDI-$(PhPA)_2$ ETL devices but still underperformed compared to devices without ETL. This occurred despite XPS and UV-vis data confirming the absence of thin film formation. As such, we hypothesize that the CBD process using NDI-$(PhBr)_2$ may have subtly altered the surface energetics or wettability of the FTO, changing perovskite crystallization and interfacial properties (Fig. S22–S23, S30 and Tables S2–S3). Photovoltaic performance metrics revealed a maximum reverse PCE of 20.90% (median 20.22%) for devices with compact TiO_2 (c-TiO_2) + mesoporous TiO_2 (mp-TiO_2) (referred to as REF), 18.69% (median 14.86%) for devices without ETL (w/o ETL), 14.92% (median 12.39%) for NDI-$(PhPA)_2$, and 16.61% (median 13.39%) for NDI-$(PhBr)_2$ (Fig. 4b); the detailed photovoltaic parameters are reported in Fig. S32 and Table S4. While ETLs typically enhance charge extraction and minimize recombination losses, the devices without ETL unexpectedly exhibited higher PCEs relative to those incorporating NDI-$(PhPA)_2$ and NDI-$(PhBr)_2$. This observation is consistent with previous studies showing that PSCs without an ETL can still achieve high efficiencies exceeding 17%.[37,38] Despite increased PCEs in some of the batches of devices that were processed, the reproducibility of performances of devices without an ETL is highly reduced and could be below 8% depending on the batch (Table S2).

Despite forming a uniform, well-anchored interlayer, NDI-$(PhPA)_2$ devices exhibited lower stabilized PCEs, primarily due to a reduction in open-circuit voltage (V_{OC}) (Fig. S32a). Given its superior molecular coverage and strong interaction with FTO, the reduced V_{OC} is likely linked to the introduction of

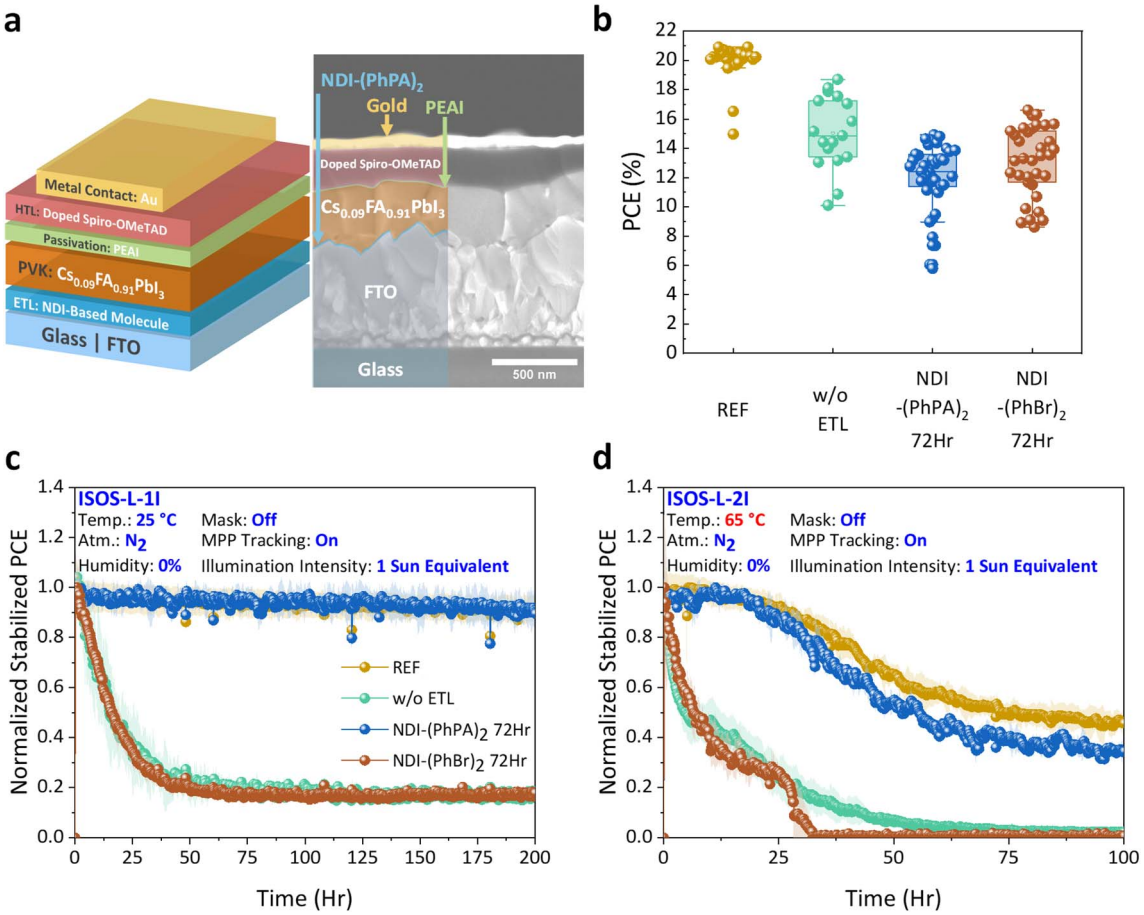

Fig. 4 Photovoltaic performance of NDI-based ETLs in PSCs. (a) Schematic and cross-sectional SEM image of the n–i–p PSC device configuration and (b) PCE from reverse *J*–*V* scans. Long-term stability of PSCs under constant simulated AM 1.5G illumination and MPPT in continuous N_2 flow at (c) 25 °C and (d) 65 °C. "REF" refers to PSCs with c-TiO_2 + mp-TiO_2 as the control ETL, while "w/o ETL" represents devices without an ETL.

suboptimal energy band alignment, generating an interfacial energy barrier with the perovskite. Contact angle measurements (Fig. S30) revealed that NDI-$(PhPA)_2$ yields a more hydrophilic surface than bare FTO yet remains less hydrophilic than the reference (c-TiO_2 + mp-TiO_2) surface. Prior studies indicate that surface polarity can influence perovskite nucleation, where more hydrophilic surfaces promote denser nucleation and smaller grains, while more hydrophobic surfaces favor fewer nucleation and larger grains.[39] Smaller grains typically result in more grain boundaries, which are often correlated with increased non-radiative recombination and reduced V_{OC}. However, since the reference devices show higher V_{OC} than NDI-$(PhPA)_2$-based devices, the V_{OC} loss is unlikely due to grain size differences and instead supports the hypothesis of an energy level mismatch at the FTO/ETL or ETL/perovskite interface. This hypothesis is further supported by cross-sectional SEM images of REF, w/o ETL, and NDI-$(PhPA)_2$ incorporated PSCs, which reveal comparable perovskite grain sizes across all devices (Fig. S31). In contrast, devices treated with NDI-$(PhBr)_2$ exhibited higher PCEs than those with NDI-$(PhPA)_2$ (Fig. 4b), which can be attributed to the lack of deposition of NDI-$(PhBr)_2$ during CBD processing, resulting in performances closer to devices without an ETL.

To evaluate the impact of NDI-based ETLs on PSC long-term stability, ISOS-L-1I and ISOS-L-2I protocols were employed.[40] Following the ISOS-L-1I testing, the devices were subjected to continuous maximum power point tracking (MPPT) under 1 sun equivalent illumination at 25 °C in an N_2 atmosphere (Fig. 4c). Current density–voltage scans were conducted every 12 hours to monitor the evolution of short-circuit current density (J_{SC}), V_{OC}, fill factor (FF), and stabilized PCE (Fig. S33). Over 200 hours of stress testing, the normalized stabilized PCE remained unchanged for both the reference (c-TiO_2 + mp-TiO_2) and NDI-$(PhPA)_2$ devices, while devices without ETL and those treated with NDI-$(PhBr)_2$ exhibited rapid and comparable degradation. Under ISOS-L-2I high-temperature stress testing at 65 °C for 100 hours, degradation accelerated for devices without ETL and those treated with NDI-$(PhBr)_2$ (Fig. 4d). Conversely, the REF and NDI-$(PhPA)_2$ devices showed greater stability. The gradual decline in normalized stabilized PCE observed in these more stable devices is likely linked to doped spiro-OMeTAD degradation, given that the ETL is the only variable and the thermal instability of doped spiro-OMeTAD is well established in the

literature.[14,16,33] These results suggest that PhPA anchoring groups in NDI-based molecules enhance device longevity by preventing interface degradation, reinforcing that NDI-$(PhPA)_2$ exhibits comparable stability to c-TiO_2 + mp-TiO_2 under both light and thermal stress conditions. In particular, devices with direct FTO-perovskite contact suffer from interface degradation due to unmitigated ion migration, surface reactions, and trap formation.[15] The impact of molecular coverage and unbound excess molecules on long-term stability was also examined in PSCs with NDI-$(PhPA)_2$ and NDI-$(PhBr)_2$ processed *via* 24-hours CBD. The unbound excess molecules refer to devices without EtOH dipping during the CBD process. Under ISOS-L-1I testing, NDI-$(PhPA)_2$ showed linear degradation, while NDI-$(PhBr)_2$ treated devices degraded rapidly. ISOS-L-2I testing further revealed that unbound NDI-$(PhPA)_2$ accelerated degradation, whereas NDI-$(PhBr)_2$ excess caused additional instability. An extended analysis is provided in SI Note 1 (Fig. S24–S29 and Tables S1–S3).

Conclusion

We employed two non-fullerene electron acceptor organic molecules with different functional groups, NDI-$(PhPA)_2$ and NDI-$(PhBr)_2$, to form ETLs in n–i–p structured PSCs. The critical role of the anchoring group in interfacial and overall device stability was assessed. Through chemical bath deposition, a thin film of NDI-$(PhPA)_2$ was deposited on an FTO substrate. The phosphonic acid group proved essential to chemical stability after the films were exposed to DMSO. This finding demonstrates that PhPA anchoring groups not only facilitate strong adhesion but also prevents molecular desorption once complete coverage is obtained. In contrast, NDI-$(PhBr)_2$ relying on weak physisorption did not adhere to FTO and was entirely removed during perovskite processing confirming its poor interfacial stability. Long-term stability assessments under ISOS-L-1I (200 hours, light stability) and ISOS-L-2I (100 hours, high-temperature light stability) protocols demonstrated that these anchoring groups play a key factor in stabilizing PSC interfaces. Films of NDI-$(PhPA)_2$ exhibited stability comparable to c-TiO_2 + mp-TiO_2, supporting its potential as a viable organic ETL. Conversely, NDI-$(PhBr)_2$-based devices degraded rapidly due to poor interfacial adhesion, effectively behaving as if no ETL was present, highlighting the need for strong molecular anchoring. These findings establish anchoring groups as key determinants of interfacial adhesion and PSC longevity. While strong interfacial bonding is essential for stability, the presence of excess unbound ETL molecules is undesirable, as they can diffuse during aging and contribute to accelerated degradation. This study reveals the importance of strategic molecular engineering in CTLs, optimizing both anchoring strength and electronic properties to develop stable, high-performance PSCs.

Conflicts of interest

There are no conflicts to declare.

Data availability

The data supporting this article have been included as part of the SI. Information on material synthesis, device fabrication protocol, characterization methods, and additional figures can be found in the SI. See DOI: **https://doi.org/10.1039/d5el00070j**.

Acknowledgements

The authors acknowledge support from the U. S. Department of Energy, Office of Science, Office of Energy Efficiency and Renewable Energy (EERE), Solar Energy Technologies Office (Award # DE-EE0009524). This work was performed in part at the Georgia Tech Institute for Electronics and Nanotechnology, a member of the National Nanotechnology Coordinated Infrastructure (NNCI), which is supported by the National Science Foundation (ECCS-2025462). S. K. and D. K. L. acknowledge the Department of Education Graduate Assistance in Areas of National need (GAANN) program at Georgia Institute of Technology (Award # 1 P200A240071). This research used the CMS 11-BM beamline of the National Synchrotron Light Source II, a U. S Department of Energy (DOE) Office Science User Facility operated for the DOE office of Science by Brookhaven National Laboratory under Contract DE-SC0012704. D. K. L. thanks the National Science Foundation Graduate Research Fellowship under Grant No. DGE-2039655 for supporting this work. Any opinion, findings, and conclusions or recommendations expressed in this material are those of the author(s) and do not necessarily reflect the views of the National Science Foundation. We thank Spencer Gilman for providing the solution UV-vis measurements of the NDI-$(PhPA)_2$ and NDI-$(PhBr)_2$ ETL molecules.

References

1 J.-P. Correa-Baena, M. Saliba, T. Buonassisi, M. Grätzel, A. Abate, W. Tress and A. Hagfeldt, *Science*, 2017, **358**, 739–744.
2 J. Y. Kim, J.-W. Lee, H. S. Jung, H. Shin and N.-G. Park, *Chem. Rev.*, 2020, **120**, 7867–7918.
3 Q. Jiang and K. Zhu, *Nat. Rev. Mater.*, 2024, **9**(6), 399–419.
4 L. Schmidt-Mende, V. Dyakonov, S. Olthof, F. Ünlü, K. M. T. Lê, S. Mathur, A. D. Karabanov, D. C. Lupascu, L. M. Herz, A. Hinderhofer, F. Schreiber, A. Chernikov, D. A. Egger, O. Shargaieva, C. Cocchi, E. Unger, M. Saliba, M. M. Byranvand, M. Kroll, F. Nehm, K. Leo, A. Redinger, J. Höcker, T. Kirchartz, J. Warby, E. Gutierrez-Partida, D. Neher, M. Stolterfoht, U. Würfel, M. Unmüssig, J. Herterich, C. Baretzky, J. Mohanraj, M. Thelakkat, C. Maheu, W. Jaegermann, T. Mayer, J. Rieger, T. Fauster, D. Niesner, F. Yang, S. Albrecht, T. Riedl, A. Fakharuddin, M. Vasilopoulou, Y. Vaynzof, D. Moia, J. Maier, M. Franckevičius, V. Gulbinas, R. A. Kerner, L. Zhao, B. P. Rand, N. Glück, T. Bein, F. Matteocci, L. A. Castriotta, A. Di Carlo, M. Scheffler and C. Draxl, *APL Mater.*, 2021, **9**(10), 109202.

5 J. Han, K. Park, S. Tan, Y. Vaynzof, J. Xue, E. W. G. Diau, M. G. Bawendi, J. W. Lee and I. Jeon, *Nat. Rev. Methods Primers*, 2025, **5**(1), 1–27.
6 H. Zhu, S. Teale, M. N. Lintangpradipto, S. Mahesh, B. Chen, M. D. McGehee, E. H. Sargent and O. M. Bakr, *Nat. Rev. Mater.*, 2023, **8**(9), 569–586.
7 Y. Rong, Y. Hu, A. Mei, H. Tan, M. I. Saidaminov, S. Il Seok, M. D. McGehee, E. H. Sargent and H. Han, *Science*, 2018, **361**(6408), eaat8235.
8 D. Zhang, D. Li, Y. Hu, A. Mei and H. Han, *Commun. Mater.*, 2022, **3**(1), 1–14.
9 J. Min, Y. Choi, D. Kim and T. Park, *Adv. Energy Mater.*, 2024, **14**, 2302659.
10 S. Shao, M. A. Loi, S. Shao and O. A. L. Photophysics, *Adv. Mater. Interfaces*, 2020, **7**, 1901469.
11 F. H. Isikgor, S. Zhumagali, L. V. Luis, M. De Bastiani, I. McCulloch and S. De Wolf, *Nat. Rev. Mater.*, 2022, **8**(2), 89–108.
12 V. M. Le Corre, M. Stolterfoht, L. Perdigón Toro, M. Feuerstein, C. Wolff, L. Gil-Escrig, H. J. Bolink, D. Neher and L. J. A. Koster, *ACS Appl. Energy Mater.*, 2019, **2**, 6280–6287.
13 G. W. Kim, H. Choi, M. Kim, J. Lee, S. Y. Son and T. Park, *Adv. Energy Mater.*, 2020, **10**, 1903403.
14 F. M. Rombach, S. A. Haque and T. J. Macdonald, *Energy Environ. Sci.*, 2021, **14**, 5161–5190.
15 D. Di Girolamo, N. Phung, F. U. Kosasih, F. Di Giacomo, F. Matteocci, J. A. Smith, M. A. Flatken, H. Köbler, S. H. Turren Cruz, A. Mattoni, L. Cinà, B. Rech, A. Latini, G. Divitini, C. Ducati, A. Di Carlo, D. Dini and A. Abate, *Adv. Energy Mater.*, 2020, **10**, 2000310.
16 Y. Yao, C. Cheng, C. Zhang, H. Hu, K. Wang, S. De Wolf, Y. Yao, C. Cheng, C. Zhang, K. Wang, H. Hu and S. De Wolf, *Adv. Mater.*, 2022, **34**, 2203794.
17 M. Morales-Masis, S. De Wolf, R. Woods-Robinson, J. W. Ager and C. Ballif, *Adv. Bioelectron. Mater.*, 2017, **3**, 1600529.
18 A. M. Soufiani, Z. Hameiri, S. Meyer, S. Lim, M. J. Y. Tayebjee, J. S. Yun, A. Ho-Baillie, G. J. Conibeer, L. Spiccia and M. A. Green, *Adv. Energy Mater.*, 2017, **7**, 1602111.
19 E. Li, C. Liu, H. Lin, X. Xu, S. Liu, S. Zhang, M. Yu, X.-M. Cao, Y. Wu, W.-H. Zhu, E. Li, C. Liu, X. Xu, S. Liu, S. Zhang, M. Yu, X. Cao, Y. Wu, W. Zhu and H. Lin, *Adv. Funct. Mater.*, 2021, **31**, 2103847.
20 S. A. Paniagua, A. J. Giordano, O. L. Smith, S. Barlow, H. Li, N. R. Armstrong, J. E. Pemberton, J.-L. Brédas, D. Ginger and S. R. Marder, *Chem. Rev.*, 2016, **116**, 7117–7158.
21 T. Bauer, T. Schmaltz, T. Lenz, M. Halik, B. Meyer and T. Clark, *ACS Appl. Mater. Interfaces*, 2013, **5**, 6073–6080.
22 J. C. Love, L. A. Estroff, J. K. Kriebel, R. G. Nuzzo and G. M. Whitesides, *Chem. Rev.*, 2005, **105**, 1103–1170.
23 D. Kim, A. W. H. Lee, J. I. Eastcott and B. D. Gates, *ACS Appl. Nano Mater.*, 2018, **1**, 2237–2248.
24 P. Silberzan, L. Leger, D. Ausserre and J. J. Benattar, *Langmuir*, 1991, **7**, 1647–1651.
25 P. J. Hotchkiss, S. C. Jones, S. A. Paniagua, A. Sharma, B. Kippelen, N. R. Armstrong and S. R. Marder, *Acc. Chem. Res.*, 2012, **45**, 337–346.
26 X. Wan, I. Lieberman, A. Asyuda, S. Resch, H. Seim, P. Kirsch and M. Zharnikov, *J. Phys. Chem. C*, 2020, **124**, 2531–2542.
27 S. Zhang, F. Ye, X. Wang, R. Chen, H. Zhang, L. Zhan, X. Jiang, Y. Li, X. Ji, S. Liu, M. Yu, F. Yu, Y. Zhang, R. Wu, Z. Liu, Z. Ning, D. Neher, L. Han, Y. Lin, H. Tian, W. Chen, M. Stolterfoht, L. Zhang, W.-H. Zhu and Y. Wu, *Science*, 2023, **380**, 404–409.
28 G. Qu, L. Zhang, Y. Qiao, S. Gong, Y. Ding, Y. Tao, S. Cai, X. Y. Chang, Q. Chen, P. Xie, J. Feng, C. Gao, G. Li, H. Xiao, F. Wang, H. Hu, J. Yang, S. Chen, A. K. Y. Jen, X. Chen and Z. X. Xu, *Nat. Commun.*, 2025, **16**(1), 1–12.
29 D. S. Utomo, L. M. Svirskaite, A. Prasetio, V. Malinauskiene, P. Dally, E. Aydin, A. Musiienko, V. Getautis, T. Malinauskas, R. Azmi and S. De Wolf, *ACS Energy Lett.*, 2024, **9**, 1682–1692.
30 X. Zhan, A. Facchetti, S. Barlow, T. J. Marks, M. A. Ratner, M. R. Wasielewski, S. R. Marder, X. Zhan, A. Facchetti, T. J. Marks, A. Ratner, M. R. Wasielewski, S. Barlow and S. R. Marder, *Adv. Mater.*, 2011, **23**, 268–284.
31 T. M. Figueira-Duarte and K. Müllen, *Chem. Rev.*, 2011, **111**, 7260–7314.
32 B. A. Jones, A. Facchetti, M. R. Wasielewski and T. J. Marks, *J. Am. Chem. Soc.*, 2007, **129**, 15259–15278.
33 S. Kim, S. Sabury, C. A. R. Perini, T. Hossain, A. O. Yusuf, X. Xiao, R. Li, K. R. Graham, J. R. Reynolds and J.-P. Correa-Baena, *ACS Energy Lett.*, 2024, **9**, 4501–4508.
34 S. L. Suraru and F. Würthner, *Angew. Chem., Int. Ed.*, 2014, **53**, 7428–7448.
35 C. Reichardt and T. Welton, *Solvents and Solvent Effects in Organic Chemistry*, Wiley, NY, 4th edn, 2011.
36 A. W. Adamson and A. P. Gast, *Physical Chemistry of Surfaces*, Wiley, NY, 6th edn, 1997.
37 H. Yu, J. Woo Lee, J. Yun, K. Lee, J. Ryu, J. Lee, D. Hwang, S. Keun Kim, J. Jang, H. Yu, J. Yun, K. Lee, J. Ryu, J. Lee, J. Jang, J. W. Lee, D. Hwang and S. K. Kim, *Adv. Energy Mater.*, 2017, **7**, 1700749.
38 H. Yu, J. Ryu, J. W. Lee, J. Roh, K. Lee, J. Yun, J. Lee, Y. K. Kim, D. Hwang, J. Kang, S. K. Kim and J. Jang, *ACS Appl. Mater. Interfaces*, 2017, **9**, 8113–8120.
39 C. Bi, Q. Wang, Y. Shao, Y. Yuan, Z. Xiao and J. Huang, *Nat. Commun.*, 2015, **6**(1), 1–7.
40 M. V. Khenkin, E. A. Katz, A. Abate, G. Bardizza, J. J. Berry, C. Brabec, F. Brunetti, V. Bulović, Q. Burlingame, A. Di Carlo, R. Cheacharoen, Y. B. Cheng, A. Colsmann, S. Cros, K. Domanski, M. Dusza, C. J. Fell, S. R. Forrest, Y. Galagan, D. Di Girolamo, M. Grätzel, A. Hagfeldt, E. von Hauff, H. Hoppe, J. Kettle, H. Köbler, M. S. Leite, S. (Frank) Liu, Y. L. Loo, J. M. Luther, C. Q. Ma, M. Madsen, M. Manceau, M. Matheron, M. McGehee, R. Meitzner, M. K. Nazeeruddin, A. F. Nogueira, Ç. Odabaşı, A. Osherov, N. G. Park, M. O. Reese, F. De Rossi, M. Saliba, U. S. Schubert, H. J. Snaith, S. D. Stranks, W. Tress, P. A. Troshin, V. Turkovic, S. Veenstra, I. Visoly-Fisher, A. Walsh, T. Watson, H. Xie, R. Yıldırım, S. M. Zakeeruddin, K. Zhu and M. Lira-Cantu, *Nat. Energy*, 2020, **5**(1), 35–49.